ACS OMEGA

Open Access

http://pubs.acs.org/journal/acsodf

Article

Investigation on the Combustion Characteristics and Environmental Effects of Hydrogen-doped Natural Gas for Domestic Water Heaters

Yiyu Chen, Liwen Long, Jie Niu, Taiming Huang, Xi Chen, Jing Zhang, Zhongmin Wan,* and Bo Yu

Cite This: *ACS Omega* 2023, 8, 48370−48380

Read Online

ACCESS | Metrics & More | Article Recommendations

ABSTRACT: The addition of hydrogen to natural gas is an effective approach to broaden the range of applications for hydrogen and address the issue of global warming. However, the inclusion of hydrogen alters the combustion properties of natural gas. The paper established a simplified mechanism consisting of 19 components and a 67-step reaction for hydrogen-doped natural gas combustion. With this simplified mechanism, the effects of hydrogen doping and the utilization of porous media combustion techniques on the combustion characteristics of natural gas were investigated numerically. The results suggested that the utilization of porous media combustion technology is beneficial for achieving the complete combustion of hydrogen-doped natural gas and reducing pollutant emissions. Additionally, the total gas cost and environmental impact of domestic gas water heaters with hydrogen-doping natural gas were estimated. The findings show that the use of 20% hydrogen-doped natural gas contributes to a decrement in fuel costs and reduced emissions of CO by 25.4%, NO_X by 53.9%, and CO_2 by 6.78%.

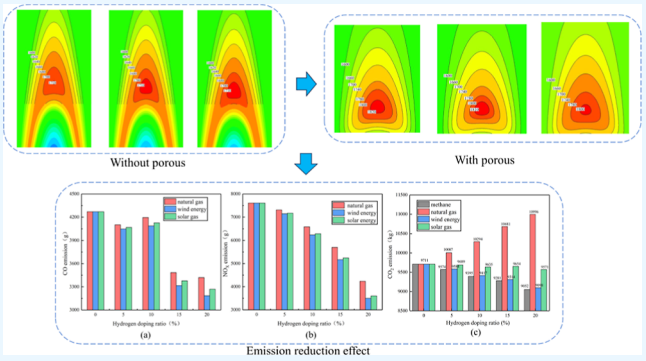

1. INTRODUCTION

With the aim of achieving carbon neutrality and sustainable development, hydrogen energy has gained considerable attention due to its benefits of being clean, carbon-free, green, efficient, and renewable.[1−3] Nonetheless, the utilization of pure hydrogen is constrained by issues such as production, storage, transportation, and end-use. One promising solution for the large-scale implementation of hydrogen energy at a low cost is blending hydrogen into the current natural gas pipeline network and transporting it to end-users.

European countries have been gradually blending hydrogen into their natural gas pipeline networks.[4,5] For example, the GRHYD project in France added 6% hydrogen to the original gas pipeline, while the HyDeploy project in the United Kingdom successfully blended 20% hydrogen into the pipeline at Kiel University. However, blending hydrogen into natural gas changes its combustion characteristics and affects the end-of-the-art equipment performance. Sun et al.[6] studied the effects of blending different proportions of hydrogen into natural gas on domestic gas appliances. The results showed that domestic gas water heaters would experience the phenomenon of backfire when the hydrogen doping ratio was 25%. Jones et al.[7] found that backfire could be avoided in round holes with a diameter of less than 3.5 mm in a UK gas appliance when the hydrogen blend was less than 34.7 mol %. Zhao et al.[8] studied the effects of blending hydrogen on the combustion and cooking performance of stove burners in the United States. It came to the conclusion that the performance of the stove burners was not significantly affected when the hydrogen blend was at 15%. Zhao et al.[9] evaluated the combustion performance of mixtures with different hydrogen blends on residential and commercial oven burners. They found that blending 25% hydrogen caused an ignition backfire. When the hydrogen blend was 10%, the burner temperature increased by 63%, but a higher blend did not significantly affect the burner surface temperature. Zhan et al.[10] studied the effect of different ratios of hydrogen-doped natural gas on the flame inside a domestic gas water heater. The results showed that as the hydrogen ratio increased, the height of the internal flame first increased and then decreased.

Numerous studies have investigated the combustion characteristics of hydrogen-doped natural gas. Kong et al.[11] studied the flame characteristics of a horizontal jet flame of mixed hydrogen and natural gas. Their results showed that the flame temperature increased after hydrogen addition. Donohoe et al.[12] examined the ignition delay time of hydrogen-doped

Received: October 8, 2023
Revised: November 22, 2023
Accepted: November 22, 2023
Published: December 6, 2023

natural gas under different temperatures, pressures, hydrogen doping ratios, and long-chain hydrocarbon contents. Their results showed that the ignition delay time decreases as the parameters increase. Li et al.[12,13] investigated the impact of hydrogen doping ratios and initial pressure on flame instability and found that blending hydrogen led to enhanced diffusion thermal instability and hydrodynamic instability, which caused flame instability. Ennetta et al.[14] simulated the laminar burning velocity of hydrogen-doped natural gas with varying hydrogen doping ratios and found that hydrogen blending increased the laminar burning velocity. If the flow velocity of the premixed gas is equal to the flame propagation speed, then the flame will remain in a stable state. However, the addition of hydrogen gas increases the flame propagation speed, causing the flame to propagate upstream toward the burner, leading to the occurrence of a dangerous phenomenon known as backfire. Lu et al.[15] conducted numerical simulations to analyze the effect of gas flow distribution on pollutant emissions from gas turbines using hydrogen-doped natural gas. Their findings indicated that the NO_X concentration gradually increased when the hydrogen doping ratio was below 40%. Pan et al.[16] simulated pollutant emissions from industrial furnaces burning hydrogen-doped natural gas and concluded that NO_X emissions decreased as the hydrogen doping ratio increased at the given combustion temperature.

The combustion performance of hydrogen-doped natural gas was often studied using numerical methods due to the flammable and explosive characteristics of hydrogen. However, the most widely accepted methane-hydrogen dynamics (GRI-Mech 3.0, USC, Aramco, and San Diego) involve dozens of components and hundreds of reactions, which makes direct calculation time-consuming.[17] If the detailed mechanism is used directly for computer calculations, it will take a long time to calculate. To reduce computational costs, researchers have simplified the mechanism through certain methods while still maintaining sufficient accuracy to simulate the reaction process. Gimeno-Escobedo et al.[18] used a direct relation graph (DRG) and direct relation graph with error propagation-aided sensitivity analysis (DRGEPSA) to simplify a mixture with a 50% hydrogen doping ratio based on GRI-Mech 3.0. They obtained a simplified mechanism of 26 components and 143 reactions, which was verified to have reasonable error. Liu et al.[19] simplified GRI-Mech 3.0 by 82% using sensitivity analysis (SA), DRG, and DRGEPSA methods. They found that the simplified combustion model had good consistency in temperature and with some components.

Compared with traditional combustion technology, porous media combustion technology has the advantages of a compact structure, better combustion stability, higher combustion efficiency, and lower pollutant emission.[20−22] Kıymaz et al.[23] investigated the effects of different wall temperatures and hydrogen blending ratios on the phenomenon of hydrogen-enriched natural gas flashback. Fruzza et al.[24] found that the occurrence of flashback in hydrogen-enriched natural gas is closely related to the flame and burner structure. Arrieta et al.[25] studied the effects of mixtures with different hydrogen doping ratios and equivalent ratios on temperature distribution, radiation efficiency, and pollutant emissions in porous media burners. Gao et al.[26] studied the influence of different porous materials on flame stability. The results showed that with the increase in thermal conductivity of foam ceramics, the flame stability limit increases, and with the increase in pore density, the flame stability limit decreases. Jia et al.[27] proposed a burner with a double-layer porous media structure and simulated the combustion performance of a methane-air mixture. The results showed that the new porous media burner can significantly reduce the emission concentration of NO_X. In summary, porous medium combustion technology has shown good performance in reducing pollutant emissions and is promised to improve the combustion characteristics of hydrogen-doped natural gas. Lamioni et al.[28] utilized a CFD model to investigate the combustion characteristics of hydrogen-enriched natural gas in perforated premixed burners. The results indicated that the blending of hydrogen gas decreases the emissions of pollutants such as CO and NO.

In this study, we explored the potential of using a porous medium structure to improve the combustion stability of hydrogen-doped natural gas and reduce pollutant emissions. To achieve this, a simplified methane-hydrogen combustion mechanism in Chemkin software using SA and DRG methods based on the GRI-Mech 3.0 mechanism was established. We then applied this simplified mechanism to a two-dimensional double-layer porous media model based on the volume averaging method and compared the temperature and pollutant emissions at different hydrogen doping ratios and equivalent ratios. Finally, we evaluated the economic and environmental performance of domestic gas water heaters that utilize hydrogen-doped natural gas and porous media combustion technology.

2. REDUCE METHOD

GRI-Mech 3.0 has been shown to simulate the combustion characteristics of pure hydrogen flames and hydrogen-rich mixtures well. In order to obtain a simplified mechanism suitable for CFD calculation, GRI-Mech 3.0 is used as the initiation mechanism of the reduction process. The simplified combustion mechanism model is based on the 0-D closed homogeneous model in Chemkin. The specific boundary conditions are selected for the reactor; for example, the operating pressure is 1 atm, the initial temperature is 1800 K, the equivalent ratio is 1.0, the hydrogen doping ratio is increased from 0 to 90%, the sampling interval is 10%, and the heat loss is ignored. The value of the parameter is taken according to the data collected during the normal operation of domestic gas water heaters.

In practice, temperature, flame stability, and pollutant emissions play a key role in the design and operation of domestic gas appliances. Laminar burning characterizes the velocity of the flame front during combustion. Also, it is one of the important parameters for studying flame stability. Ueda et al.[29] show that there is a good linear relationship between laminar burning velocity and (H + OH) concentration maximum for CH_4/H_2 mixtures. Therefore, in the reduction process, the maximum temperature, the maximum and end point of H and OH primitives, and the endpoint of CO and NO_X are selected as the target flame characteristics to drive the reduction of the mechanism.

In the simplification process, key basic components (CH_4, H, H_2, O, O_2, OH, N_2, NO, and NO_2) and reaction products (CO, CO_2, and H_2O) are searched as the initial components. Next, a framework mechanism is obtained by using DRG and DRGEP. Furthermore, the SA of the framework mechanism is carried out to obtain the final simplified mechanism. The absolute error and relative error are set to 10×10^{-6} and 10%, respectively. The DRG operation reduces the original mechanism to 20 components and 81 reactions, and the

https://doi.org/10.1021/acsomega.3c07418
ACS Omega 2023, 8, 48370−48380

DRGEP operation continues to simplify, further reducing the mechanism to 19 components, a 67-step reaction mechanism. As shown in Table 1, the final maximum error value of the

Table 1. Target Error Parameter

components and temperature	error (%)
CO	0
NO	0
NO_2	0.0
temperature	0.8
H	36.4
OH	1.0

simplified mechanism by DRG and DRG is 36.4% of that of the H radical, which represents a large error in the laminar burning velocity. Therefore, the SA of the H radical is carried out, and the error of laminar burning velocity is reduced by modifying the pre-exponential constants of the reaction with the largest sensitivity coefficient of the H radical.

As shown in Figure 1, in the analysis of H radical sensitivity of 0.8 and 1.0, #34 reaction: OH + CO ↔ H + CO_2 is one of the ten reactions with the greatest influence on H radical. And the pre-exponential constant of #34 is selected for modification. Besides, #38 reaction: CH_2 + O_2 → H + OH + CO is one of the ten reactions with the greatest influence on H radical in the analysis of H radical sensitivity of 1.2 and 1.4. Therefore, the pre-exponential constant of #38 is selected for modification.

The comparison model uses a set of one-dimensional laminar premixed flame models and finally obtains the relative data of the premixed fuel-air mixture with an equivalent ratio of 0.8−1.2. When the equivalent ratio is 0.8, 1.0, and 1.2, the error of the components is less than 10%, as shown in Figure 2a and the flame speed is less than 6%, as shown in Figure 2b.

3. NUMERICAL MODELS

3.1. Physical Model. As shown in Figure 3, this paper establishes a physical model of a double-layer porous layer in Fluent software. By creating two separate, two-layer 60 mm fluid domains as the filling regions of the porous medium. The burner cylinder has an inner diameter of 50 mm and a total length of 150 mm, and two layers of 60 mm porous medium area are filled inside as the preheating zone and combustion zone. Alumina balls are used in the preheating zone, zirconia foam ceramic is used in the combustion zone, and the parameters of the porous mediums are shown in Table 2.

3.1.1. Mathematical Model. In order to save computer resources, this paper simplified the physical model of a three-dimensional axis-symmetric structure to a two-dimensional structure. For the convenience of computation, this article

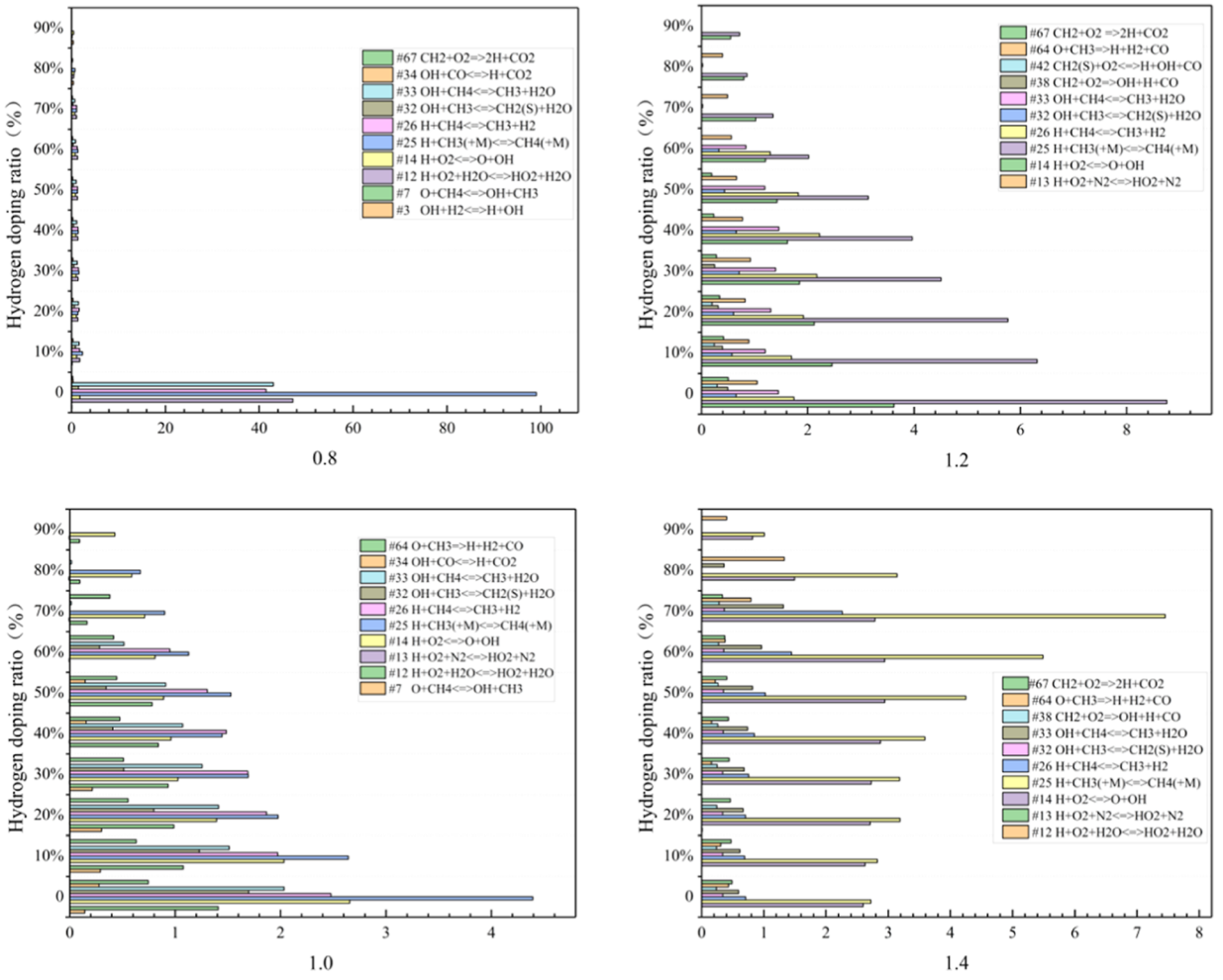

Figure 1. SA of H primitives when the equivalent ratio is 0.8−1.4.

https://doi.org/10.1021/acsomega.3c07418
ACS Omega 2023, 8, 48370−48380

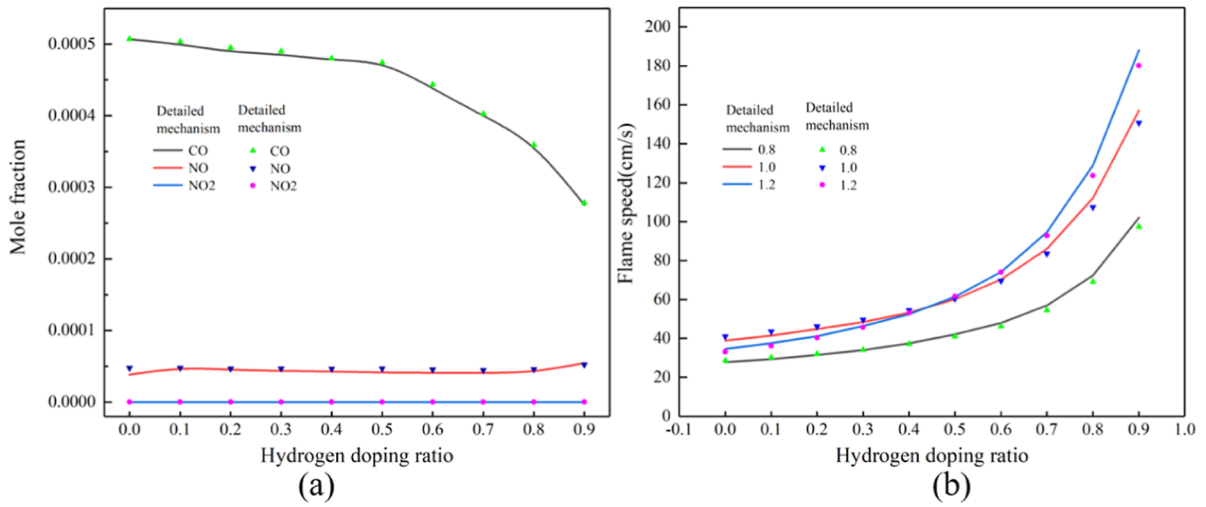

Figure 2. Comparison of (a) mole fraction of the pollution components (the equivalent ratio is 0.8) and (b) flame speed from the detailed and the simplified mechanisms (the equivalent ratio is 0.8, 1.0, and 1.2).

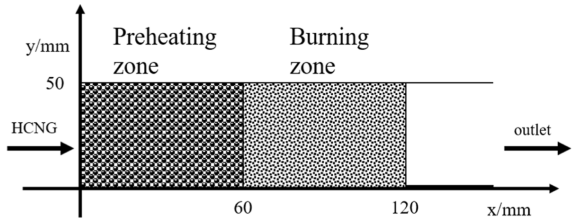

Figure 3. Physical model of double-layer porous media.

Table 2. Physical Property Parameters of Porous Media Materials

parameters	preheat zone	combustion zone
materials	Al_2O_3	ZrO_2
density (kg m^{-3})	3440	3750
specific heat (J kg^{-1} K^{-1})	710	570
PPI		10
porosity	0.265	0.8
effective thermal conductivity (W m^{-1} K^{-1})	1.87	0.41

introduces some reasonable assumptions in the process of numerical calculation.[30]

(1) Ignore the radiation effect of the gas;
(2) The gas is an incompressible ideal gas and is fully premixed;
(3) The porous medium is inert and isotropic;
(4) The gas and the solid are in a state of thermal equilibrium.

The relevant control equations covered in this work are as follows

Continuity equation

$$\frac{\partial(\varepsilon\rho U)}{\partial \mathcal{X}} + \frac{\partial(\varepsilon\rho V)}{\partial \mathcal{Y}} = 0 \tag{1}$$

where ε is the porosity of the porous medium; ρ is the average density of the mixed gas; U is the axial gas velocity; and V is the longitudinal gas velocity.

Momentum equation

$$\frac{\partial(\varepsilon\rho UU)}{\partial \mathcal{X}} + \frac{\partial(\varepsilon\rho UV)}{\partial \mathcal{Y}} = -\frac{\partial P}{\partial \mathcal{X}} + \frac{\partial}{\partial \mathcal{X}}\left(\mu\frac{\partial U}{\partial \mathcal{X}}\right) + \frac{\partial}{\partial \mathcal{X}}\left(\mu\frac{\partial U}{\partial \mathcal{Y}}\right) + \frac{\Delta P}{\Delta \mathcal{X}} \tag{2}$$

$$\frac{\partial(\varepsilon\rho UV)}{\partial \mathcal{X}} + \frac{\partial(\varepsilon\rho VV)}{\partial \mathcal{Y}} = -\frac{\partial P}{\partial \mathcal{Y}} + \frac{\partial}{\partial \mathcal{X}}\left(\mu\frac{\partial V}{\partial \mathcal{X}}\right) + \frac{\partial}{\partial \mathcal{Y}}\left(\mu\frac{\partial V}{\partial \mathcal{Y}}\right) + \frac{\Delta P}{\Delta \mathcal{Y}} \tag{3}$$

where P is the pressure and μ is the viscosity.

Energy equation

$$\frac{\partial(\varepsilon\rho Uh)}{\partial \mathcal{X}} + \frac{\partial(\varepsilon\rho Vh)}{\partial \mathcal{Y}} = \frac{\partial}{\partial \mathcal{X}}\left(k_{\text{eff}}\frac{\partial T_g}{\partial \mathcal{X}}\right) + \frac{\partial}{\partial \mathcal{Y}}\left(k_{\text{eff}}\frac{\partial T_g}{\partial \mathcal{Y}}\right) + \varepsilon\sum_{i=1}^{N} h_i w_i W_i - \varepsilon\frac{\partial}{\partial \mathcal{X}}\left[\sum_{i=1}^{N} Y_i h_i D_{im}\frac{\partial(pY_i)}{\partial \mathcal{X}}\right] - \varepsilon\frac{\partial}{\partial \mathcal{Y}}\left[\sum_{i=1}^{N} Y_i h_i D_{im}\frac{\partial(pY_i)}{\partial \mathcal{Y}}\right] \tag{4}$$

where k_{eff} is the effective thermal conductivity; T_g is the temperature of the gas mixture; h_i is the molar enthalpy of species i; w_i is the molar yield of species i; W_i is the relative molecular mass of species i; Y_i is the mass fraction of species i; D_{im} is the mass diffusion coefficient of the gas.

Species transport equation

$$\frac{\partial(\varepsilon\rho UY_i)}{\partial \mathcal{X}} + \frac{\partial(\varepsilon\rho VY_i)}{\partial \mathcal{Y}} = \frac{\partial}{\partial \mathcal{X}}\left[\varepsilon D_{im}\frac{\partial(\rho Y_i)}{\partial \mathcal{X}}\right] + \frac{\partial}{\partial \mathcal{Y}}\left[\varepsilon D_{im}\frac{\partial(\rho Y_i)}{\partial \mathcal{Y}}\right] + \varepsilon w_i W_i \tag{5}$$

Ideal gas state equation

$$P = \frac{\rho RT}{\bar{W}} \tag{6}$$

https://doi.org/10.1021/acsomega.3c07418
ACS Omega 2023, 8, 48370−48380

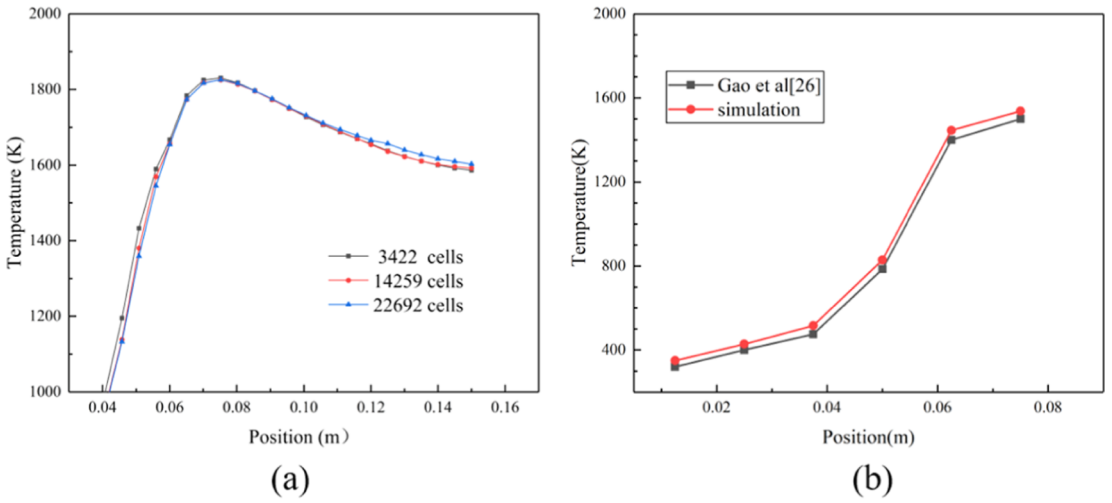

Figure 4. (a) Central axis temperature with different grid cells. (b) Verification of numerical values and experimental results.

where $\bar{W}$ is the average molecular weight of the gas mixture.

The equivalent ratio is defined as the ratio of the actual fuel/oxygen mixing ratio to the fuel/oxygen mixing ratio under chemical equivalent conditions, which is defined as follows

$$\phi = \frac{\left(\frac{F}{A}\right)_{\text{actual}}}{\left(\frac{F}{A}\right)_{\text{theory}}} \tag{7}$$

Reynolds number

$$Re = \frac{\rho UD}{\mu} \tag{8}$$

D and μ represent the average diameter of the porous medium and the viscosity of the fluid, respectively.

The empirical formula for viscous resistance and inertial resistance of a porous media-filled bed with foamed ceramics[30,31]

$$C_1 = \frac{150(1-\varepsilon)^2}{{d_p}^2\varepsilon^3} \tag{9}$$

$$C_2 = \frac{1.75(1-\varepsilon)}{d_p\varepsilon^3} \tag{10}$$

$$C_1 = \frac{150(1-\varepsilon)n^2}{0.0254^2\varepsilon^3} \tag{11}$$

$$C_2 = \frac{3.5n\sqrt{1-\varepsilon}}{0.0254\varepsilon^3} \tag{12}$$

Formulas 9 and 10 represent the viscous drag coefficient of alumina balls, and formulas 11 and 12 represent the resistance coefficient of foam ceramics. Kuwahara et al.[32] believe that in the flow of porous media, when $Re > 80$, turbulence effects cannot be ignored, and when $Re > 160$, turbulence effects must be considered. Therefore, the realizable $k-\varepsilon$ turbulence model is chosen. The inlet velocity and pressure outlet boundary conditions. In addition, the heat transfer condition of the outer wall is set to a mixed heat transfer of radiation and convection; the normal emissivity of the inner wall and outer wall is 0.8,[33] and the heat transfer coefficient of the wall surface is 20 W/(m^2 K). The heat transfer expression is

$$q = h_c(T_W - T_\infty) + \varepsilon_s\sigma(T_W^4 - T_\infty^4) \tag{13}$$

h_c represents the convective heat transfer coefficient between the combustion chamber wall and the environment, T_w and T_∞ represent the outer wall temperature and ambient temperature, respectively, ε_s is the emissivity of the combustion chamber wall, and the Stepan−Boltzmann constant σ is 5.67×10^{-8} W/(m^2 K^4).

3.2. Numerical Simulation Validation. In order to save computer resources and improve the calculation accuracy, the mesh numbers of 3422, 14,259, and 22,692 cells are selected for simulation. Figure 4 shows the central axis temperatures for three different mesh accuracies. Overall, the temperature trend of the central axis predicted by the three meshes of different accuracy is consistent. However, according to Figure 4a, the maximum temperature difference of the central axis of 3422 cells is about 73 K, with an error of about 5%. While the maximum difference in temperature for 14,259 cells is about 24 K, and the error is about 1.5% compared to the prediction of 22,692 cells. Therefore, the number of 14,259 cells is significantly better than the number of 3422 cells. Taking into account computer resources, this paper selects 14,259 cells for grid calculation.

In order to verify the reliability and accuracy of the mechanism and porous media combustion model, the central axis temperature is compared with detailed experimental results. Gao et al.[26] conducted experiments on methane/air combustion in porous media. The diameter of the porous medium combustion is 50 mm, and the length is 200 mm. The outer wall of the burner is filled with Kaowool, which serves as insulation and multiple thermocouples are inserted in the middle of the porous medium to measure the center temperature. This article selects ZrO_2 foam from the Gao experiment for verification. Figure 4b shows that under the combustion condition of an inlet velocity of 0.3 m/s and an equivalent ratio of 0.6, the numerical calculation results are basically consistent with the experimental results of Gao et al.[26] In terms of other characteristics, the simulation results are in good agreement with the experimental results. Therefore, the model meets the requirements of engineering applications.

https://doi.org/10.1021/acsomega.3c07418
ACS Omega 2023, 8, 48370−48380

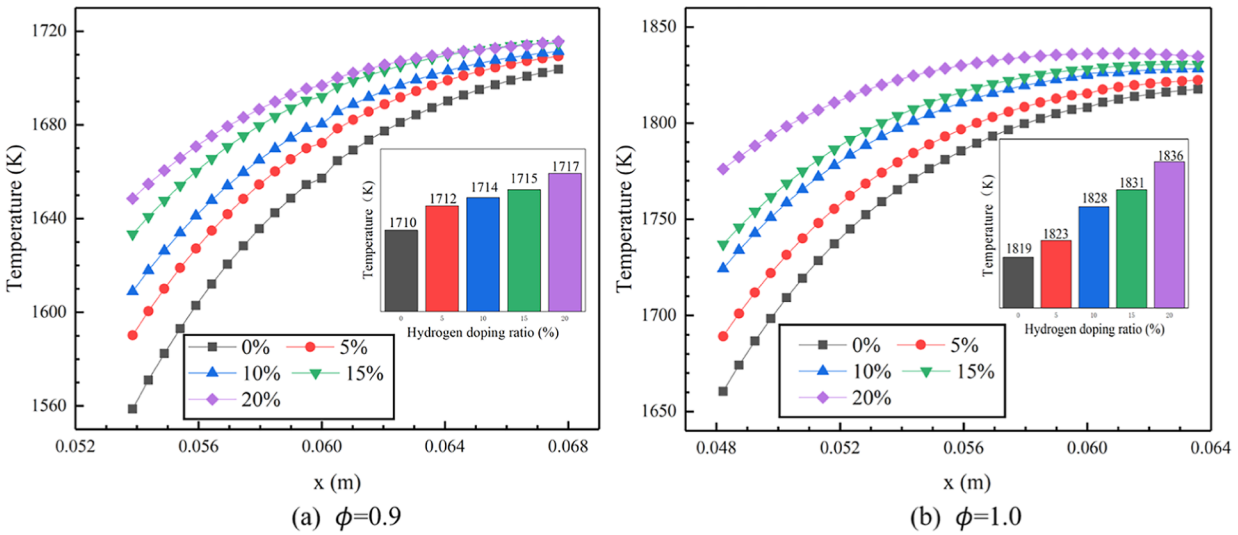

Figure 5. Central axis temperature of 0−20% hydrogen doping ratio. (a) Equivalent ratio is 0.9, and (b) equivalent ratio is 1.0.

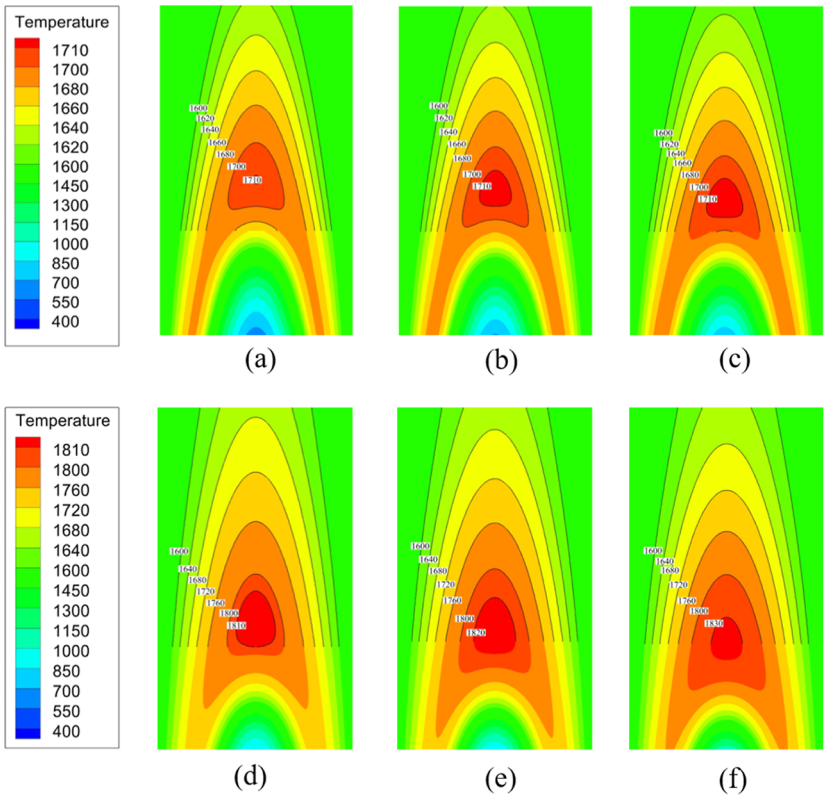

Figure 6. Two-dimensional temperature distribution of the 0/10/20% hydrogen doping ratio when the equivalent ratio is 0.9: (a) 0% H_2; (b) 10% H_2; (c) 20% H_2/the equivalent ratio is 1.0; (d) 0% H_2; (e) 10% H_2; and (f) 20% H_2.

4. RESULTS AND DISCUSSION

4.1. Effect of Hydrogen Doping on Temperature.

Figure 5 shows the maximum central axis temperature distribution of the burner when the equivalent ratios are 0.9 and 1.0 and the hydrogen doping ratio is 0−20%. As shown in Figure 5a, when the proportion of hydrogen increases from 0 to 20%, the peak temperature of the flame increases from 1710 to 1717 K when the equivalent ratio is 0.9. As shown in Figure 5b, when the equivalent ratio is 1.0, the peak temperature of the flame increases from 1819 K with a hydrogen doping ratio of 0 to 1836 K with a hydrogen doping ratio of 20%. Figure 6 shows a two-dimensional temperature distribution with equivalent ratios of 0.9 and 1.0 and hydrogen doping ratios of 0, 10, and 20%. In Figure 6b, the temperature contour of 1710 K is positioned slightly earlier than that in Figure 6a. In Figure 6e, the temperature contour of 1820 K is slightly ahead of that in Figure 6d.

Since hydrogen has 1 H−H chemical bond (activation energy is 436 kJ/mol), CH_4 has 4 C−H chemical bonds (activation energy is 414 kJ/mol). The activation energy consumed by hydrogen when participating in the reaction is less than CH_4, so the chemical properties of hydrogen are

https://doi.org/10.1021/acsomega.3c07418
ACS Omega 2023, 8, 48370−48380

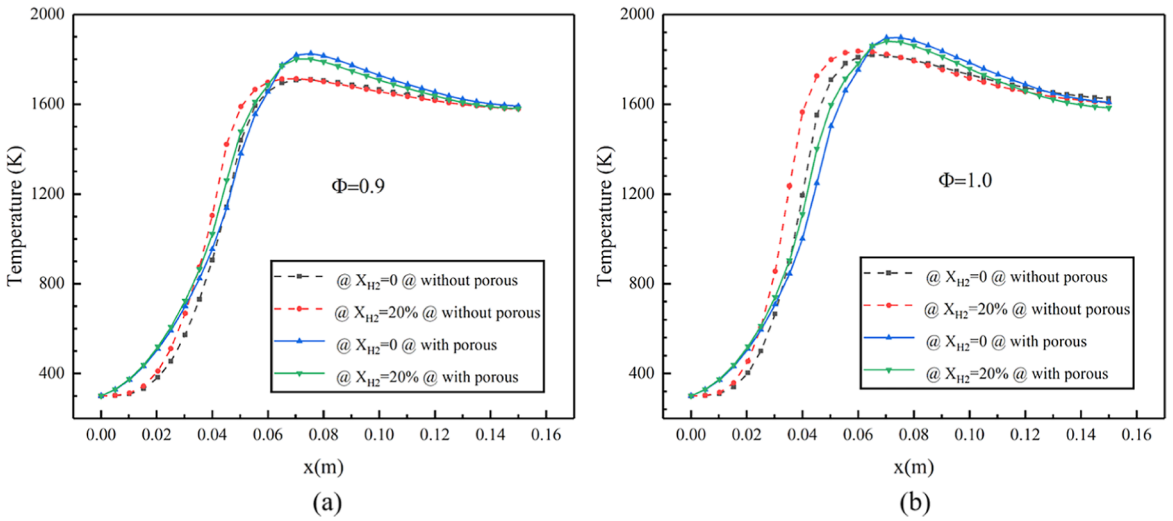

Figure 7. Effect of porous medium on the temperature of the central axis of the 0/20% hydrogen doping ratio. (a) Equivalent ratio is 0.9, and (b) equivalent ratio is 1.0.

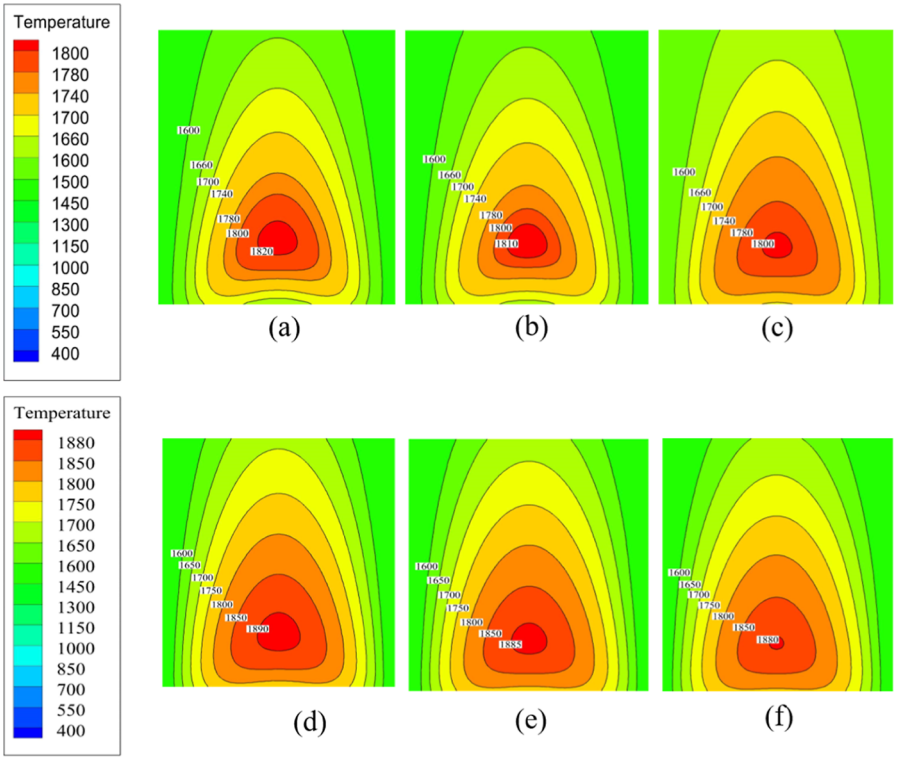

Figure 8. Two-dimensional temperature distribution of the 0/10/20% hydrogen doping ratio in the porous medium when the equivalent ratio is 0.9: (a) 0% H_2; (b) 10% H_2; (c) 20% H_2/the equivalent ratio is 1.0; (d) 0% H_2; (e) 10% H_2; and (f) 20% H_2.

more active and easier to react with O_2, so with the increase in the hydrogen doping ratio, the combustion exothermic reaction will occur earlier. Therefore, the initial reaction location will be closer to the fuel inlet, which is consistent with the research of Fruzza et al.[24] The advance of the initial reaction position will make the reaction more complete; the exothermic heat of the reaction will also increase; and the peak temperature of the flame will also increase.

4.2. Effect of Porous Media Structure on Temperature of Hydrogen-Doped Natural Gas. Figure 7 shows the temperature distribution of the central axis of combustion of a mixture with a hydrogen doping ratio of 0 and 20% in a burner without porous media and a burner with a porous medium at equivalent ratios of 0.9 and 1.0. As shown in Figure 7a,b, the utilization of the porous media structure will increase the peak temperature of the hydrogen-doped natural gas flame, the location of the initial reaction will be advanced, and the position of the peak temperature will be lagged. Figure 8 shows the two-dimensional temperature distribution of hydrogen-doped natural gas with a hydrogen doping ratio of 0, 10, and 20% when burned in a burner with porous media at an equivalent ratio of 0.9 and 1.0. The peak temperature (1800 K) of the 20% hydrogen doping ratio is lower than that of the 0 doped ratios in a porous medium structure.The result at an

https://doi.org/10.1021/acsomega.3c07418
ACS Omega 2023, 8, 48370−48380

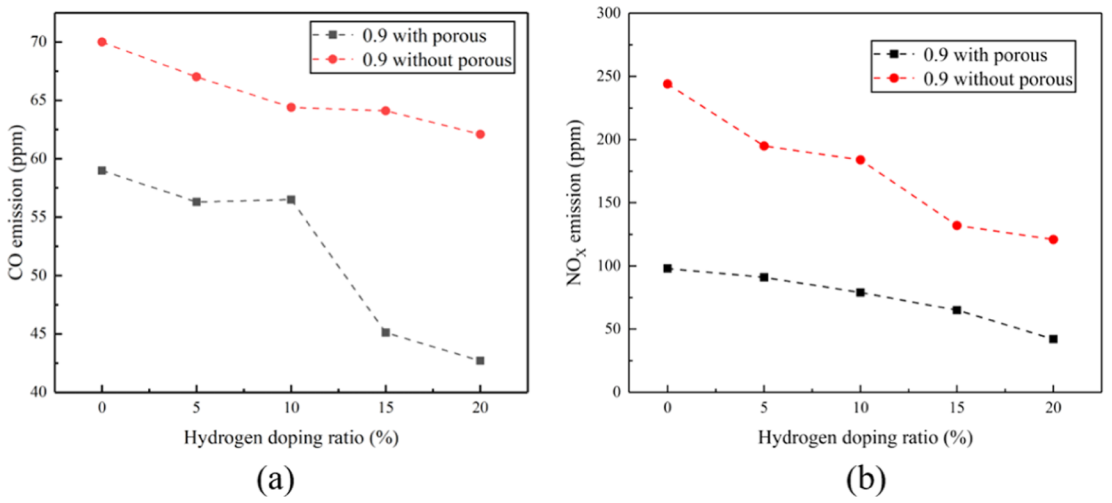

Figure 9. Effect of porous media on NO_X emissions with different hydrogen doping ratios when the equivalent ratio is 0.9−1.0.

equivalent ratio of 1.0 shares a similar trend, as shown in Figure 8.

The addition of porous media structure will preheat the fuel to make it easier to burn completely, and in terms of the macroscopic calorific value of methane and hydrogen, the calorific value of CH_4 (39.83 MJ/m^3) is higher than that of hydrogen (12.70 MJ/m^3), so as the mixing amount of hydrogen gradually increases, the temperature of complete combustion of the mixture decreases. The lag of the peak temperature position lies in the existence of the porous medium preheating section because the porosity of the preheating section will be lower than that of the combustion section, which makes the tempering of hydrogen-doped natural gas more difficult to occur due to the phenomenon of backfire, so that the peak temperature is stable at the junction of the porous medium.

4.3. Emissions of Pollutants. Figure 9 shows the emission of CO and NO_X of hydrogen-doped natural gas free flame at an equivalent ratio of 0.9 and the emissions of CO and NO_X of hydrogen-doped natural gas burning in a porous medium at an equivalent ratio of 0.9. As shown in Figure 9, the emissions of CO and NO_X decrease when the hydrogen doping ratio increases from 0 to 20%, regardless of whether the burner is filled with porous media or not.

The reason is that as the proportion of hydrogen doping increases, the C content in the fuel decreases, while the addition of hydrogen generates H and OH radicals that promote the conversion of CO to CO_2. This is consistent with the research results of Zhan et al.[10]

The reason is that the influence of temperature plays a dominant role in determining the production of thermal NO_X. When the temperature is higher than 1800 K, the amount of NO_X generated increases sharply as the temperature increases. In this study, the gas is completely premixed, and the equivalent ratio of 0.9 is more abundant than oxygen, which means that oxygen enrichment brings a larger primary air volume, which is equivalent to a certain heat dilution in the burner so that the temperature drops and the emission of NO_X decreases. This is consistent with the research results of Sun et al.[6] In the burner with added porous medium, with the increase in hydrogen doping ratio, the emission of NO_X is lower than those of unfilled burners because the hydrogen-doped natural gas burned in the porous medium will decrease in temperature with the increase in hydrogen doping ratio, thereby reducing the emission of thermal NO_X. Another reason is that the presence of porous media makes the combustion area more uniform and inhibits the thermal NO_X generated by the local high temperature.

5. ECONOMIC AND ENVIRONMENTAL ASSESSMENT

The use of hydrogen-doped natural gas can reduce the consumption of fossil energy and the emission of pollutants. In order to apply it to household gas appliances, it is necessary to analyze its economic and environmental benefits. Table 3 shows the CO and NO_X emissions from three different hydrogen production methods: natural gas reforming, wind energy hydrogen production, and solar energy hydrogen production.

Table 3. Emissions of CO and NO_X During the Hydrogen Production Process[34]

	hydrogen production from natural gas total emissions	hydrogen production from wind energy total emissions	hydrogen production from solar energy total emissions
CO (g/MJ)	0.033	0.0142	0.021
NO_X (g/MJ)	0.0761	0.0169	0.0251

5.1. Economic Evaluation. Assuming that the annual usage time is 17,520 min every year.[6] According to Chinese standard ⟨⟨GB/T 17905-2008⟩⟩,[35] the service life of domestic gas water heaters is 8 years. In this process, the gas consumption and economic comparison of burners burning methane without porous media and burning 20% hydrogen-doped methane in porous media are studied. The thermal power produced by pure methane burning is 21 kW, while the hydrogen-doped natural gas burning with a 20% hydrogen doping ratio is 18 kW. Considering that the calorific value of the gas changes with the proportion of hydrogen doping, the speed of the gas increases in order to achieve the same thermal power. The speed of 20% hydrogen-doped natural gas should be 0.348 m/s, and the burner will not experience the phenomenon of backfire. As shown in Figure 10a, the methane consumption for 8 years is 5533 m^3 without hydrogen doping, while 4606 m^3 of methane and 1151 m^3 of hydrogen will be used when the heaters use a 20% hydrogen doping ratio

https://doi.org/10.1021/acsomega.3c07418
ACS Omega 2023, 8, 48370−48380

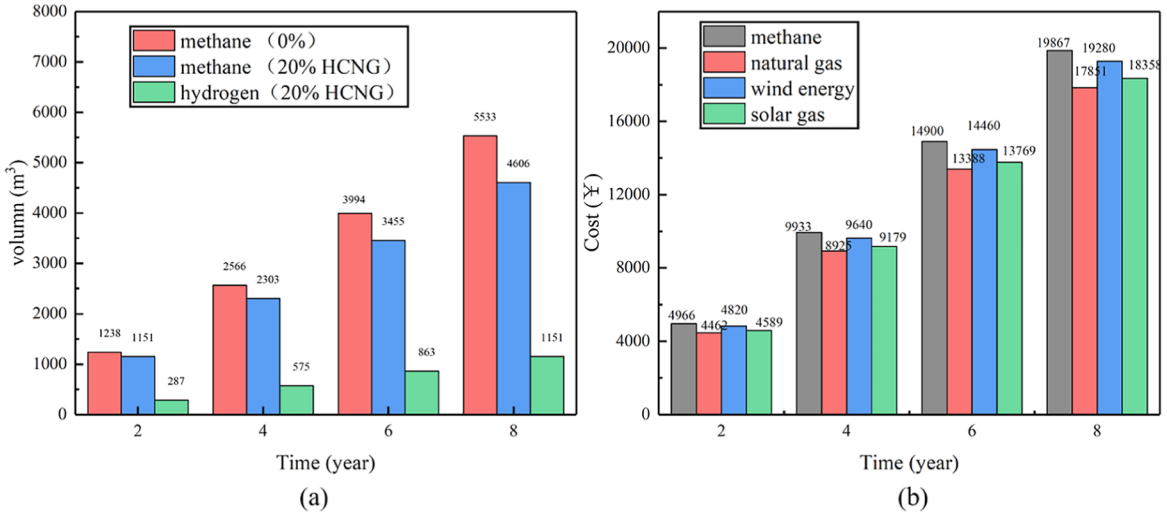

Figure 10. (a) 0 and 20% doping ratio for methane and hydrogen dosage; (b) the total cost of the three different hydrogen production methods.

mixture. Table 4 shows the price of hydrogen for three different hydrogen production methods of natural gas reforming, wind hydrogen production, and solar hydrogen production.[36] Figure 10b shows the price of hydrogen-doped natural gas using 20% hydrogen from three different hydrogen sources versus pure methane. In contrast, the cost of a gas water heater that burns pure methane is 19,867 ¥ over the entire period of use. In general, the use of hydrogen in three different hydrogen production methods at this stage can reduce the price of gas use, while among the other three methods, the price of hydrogen produced by natural gas is the lowest, at 17,851 ¥, with a decrease of about 8.6%. According to statistics,[37] the sales of gas water heaters in China in 2022 were 11.6 million units. If all of them were converted to hydrogen-doped natural gas with 20% hydrogen content, it is expected to reduce the cost by 2.9 billion ¥ per year.

Table 4. Price of Methane and Hydrogen[36]

hydrogen production	methane	natural gas	wind energy	solar energy
price (¥/m^3)	3.45	1.7	2.95	2.41
CO_2 emission (kg/m^3 H_2)		1.6875	0.04	0.45

5.2. CO Emissions. Based on the calculated model, the emission of the CO from the mixture with the ratio of 0−20% hydrogen doping and the CO emissions in the hydrogen production process of three different hydrogen production methods were studied. As shown in Figure 11a, as the proportion of hydrogen doping increases, the sum of CO emissions in the three hydrogen production processes produced by combustion decreases. If the mixture with a hydrogen doping ratio of 20% is passed at a speed of 0.3 m/s in this burner, the CO produced is 3186 g, which is 25.4% lower than the CO emissions of pure methane. According to statistics, the sales of gas water heaters in China in 2022 were 11.6 million units. If this batch of water heaters is all converted to burning 20% hydrogen mixed with natural gas, it is expected to reduce 9.8 × 10^6 kg of CO emissions.

5.3. NO_X Emissions. Based on the calculated model, the sum of NO_X emissions of a mixture with a hydrogen doping ratio of 0−20% and the production by three different hydrogen production methods are studied. As shown in Figure 11b, with the increase in the proportion of hydrogen doping, the total NO_X emissions in the three hydrogen production processes and produced by combustion decrease. When hydrogen produced from wind energy is used in burners, the NO_X emissions are minimal. If a mixture with a hydrogen doping ratio of 20% is passed at a speed of 0.3 m/s in this burner, the emission of NO_X is 3265 g, which is 53.9% lower compared to

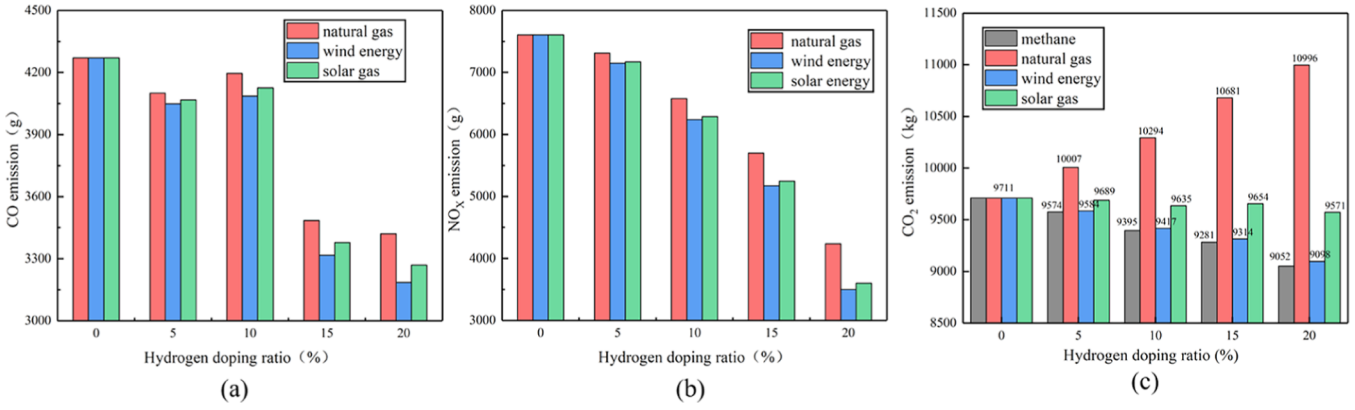

Figure 11. Emission of porous medium burner and ordinary burner operating for 2236 h. (a) CO; (b) NO_X; and (c) CO_2.

https://doi.org/10.1021/acsomega.3c07418
ACS Omega 2023, 8, 48370−48380

pure methane. According to the above method, it is expected to reduce 4.72×10^7 kg of NO emissions.

5.4. CO_2 Emissions. As shown in Table 4, the emissions of CO_2 in the three hydrogen production processes are compared. Using a burner model with porous media as an example, CO_2 emissions from three different sources of hydrogen are compared. As shown in Figure 11c, the use of hydrogen-doped natural gas will reduce carbon emissions with a decrease of 6.7%. However, taking the burner model with porous media as an example, the carbon emissions of hydrogen from three different sources have increased to varying degrees, among which the use of wind power to produce hydrogen has the lowest carbon emissions, and the use of natural gas reforming to produce hydrogen has the highest carbon emissions. According to the above method, it is expected to reduce 7.11×10^6 kg of CO_2 emissions.

6. CONCLUSIONS

In this paper, a methane−hydrogen mixture combustion mechanism was established by SA and a direct relationship diagram, according to the detailed mechanism of GRI-Mech 3.0. The CFD model was used to study the combustion characteristics of hydrogen-doped natural gas in the porous media model. The economics, as well as the environmental effect, of hydrogen-doped natural gas with different hydrogen doping ratios based on three different hydrogen production methods were discussed. The main results are as follows:

1 A simplified mechanism with a 19-component, 67-step can be well applied to the equivalent ratio of 0.8−1.4 of hydrogen-doped natural gas was obtained, and it has been verified that the predictive error of the model is no more than 10%.

2 The peak temperature of hydrogen-doped natural gas will increase with the increase in hydrogen doping ratio, and the reaction position will advance with the increase in hydrogen doping ratio. When hydrogen-doped natural gas is applied to the porous medium structure, the peak temperature will decrease with the increase in the hydrogen doping ratio.

3 The fuel cost will decrease to a certain extent after using three different ways of producing hydrogen. Also, the utilization of 20% hydrogen-doped natural gas contributes to a decrement in fuel costs and reduced emissions of CO by 25.4%, NO_X by 53.9%, and CO_2 by 6.78%.

AUTHOR INFORMATION

Corresponding Author

Zhongmin Wan − *College of Mechanical Engineering, Hunan Institute of Science and Technology, Yueyang 414006, China*; Email: zhongminwan@hotmail.com

Authors

Yiyu Chen − *College of Mechanical Engineering, Hunan Institute of Science and Technology, Yueyang 414006, China*

Liwen Long − *College of Mechanical Engineering, Hunan Institute of Science and Technology, Yueyang 414006, China*; orcid.org/0009-0006-3112-8017

Jie Niu − *College of Mechanical Engineering, Hunan Institute of Science and Technology, Yueyang 414006, China*

Taiming Huang − *College of Mechanical Engineering, Hunan Institute of Science and Technology, Yueyang 414006, China*

Xi Chen − *College of Mechanical Engineering, Hunan Institute of Science and Technology, Yueyang 414006, China*

Jing Zhang − *College of Mechanical Engineering, Hunan Institute of Science and Technology, Yueyang 414006, China*

Bo Yu − *College of Mechanical Engineering, Beijing Institute of Petrochemical Technology, Beijing 102400, China*; orcid.org/0000-0002-4231-6914

Complete contact information is available at: https://pubs.acs.org/10.1021/acsomega.3c07418

Author Contributions

Yiyu Chen: Conceptualization, Methodology, Writing—review and editing, Funding acquisition. Liwen Long: Conceptualization, Writing−review and editing. Jie Niu: Data curation, Validation. Taiming Huang: Software, Investigation. Xi Chen: Investigation, Funding acquisition. Jing Zhang: Investigation, Validation. Zhongmin Wan: Conceptualization, Methodology, Supervision, Funding acquisition, Project administration. Bo Yu: Supervision, Project administration.

Notes

The authors declare no competing financial interest.

ACKNOWLEDGMENTS

The author's portion of this work was supported by the National Key R&D Program of China (2021YFB4001604).

NOMENCLATURE

ε	porosity of porous medium
ρ	average density of the mixed gas, kg m^3
U	axial gas velocity, m s^{-1}
V	longitudinal gas velocity, m s^{-1}
P	pressure, Pa
μ	viscosity, kg m^{-1} s^{-1}
k_{eff}	effective thermal conductivity, W (m K)$^{-1}$
T_g	temperature of the gas mixture, K
h_i	molar enthalpy of species i
w_i	molar yield of species i
W_i	relative molecular mass of species i
Y_i	mass fraction of species i
D_{im}	mass diffusion coefficient of the gas, m^2 s^{-1}
$\overline{W}$	average molecular weight of the gas mixture, g mol^{-1} m
D	average diameter of the porous medium, m
h_c	convective heat transfer coefficient, W (m K)$^{-1}$
T_w	outer wall temperature, K
T_∞	ambient temperature, K
ε_s	emissivity of the combustion chamber wall
σ	Stepan−Boltzmann constant, W (m^2 K^4)$^{-1}$

REFERENCES

(1) Chen, L.; Msigwa, G.; Yang, M. Y.; Osman, A. I.; Fawzy, S.; Rooney, D. W.; Yap, P. S. Strategies to achieve a carbon neutral society: a review. *Environ. Chem. Lett.* **2022**, *20* (4), 2277−2310.

(2) Yang, S.; Yang, D. Z.; Shi, W.; Deng, C. C.; Chen, C. B.; Feng, S. J. Global evaluation of carbon neutrality and peak carbon dioxide emissions: current challenges and future outlook. *Environ. Sci. Pollut. Res.* **2022**, *30*, 81725−81744.

(3) Wang, X. Y.; Khurshid, A.; Qayyum, S.; Calin, A. C. The role of green innovations, environmental policies and carbon taxes in achieving the sustainable development goals of carbon neutrality. *Environ. Sci. Pollut. Res.* **2022**, *29* (6), 8393−8407.

(4) Mahajan, D.; Tan, K.; Venkatesh, T.; Kileti, P.; Clayton, C. R. Hydrogen Blending in Gas Pipeline Networks-A Review. *Energies* **2022**, *15* (10), 3582.

(5) Blokland, H.; Sweelssen, J.; Isaac, T.; Boersma, A. Detecting hydrogen concentrations during admixing hydrogen in natural gas grids. *Int. J. Hydrogen Energy* **2021**, *46* (63), 32318−32330.
(6) Sun, M. X.; Huang, X. M.; Hu, Y. L.; Lyu, S. Effects on the performance of domestic gas appliances operated on natural gas mixed with hydrogen. *Energy* **2022**, *244*, 122557.
(7) Jones, D. R.; Al-Masry, W. A.; Dunnill, C. W. Hydrogen-enriched natural gas as a domestic fuel: an analysis based on flash-back and blow-off limits for domestic natural gas appliances within the UK. *Sustain. Energy Fuels* **2018**, *2* (4), 710−723.
(8) Zhao, Y.; McDonell, V.; Samuelsen, S. Influence of hydrogen addition to pipeline natural gas on the combustion performance of a cooktop burner. *Int. J. Hydrogen Energy* **2019**, *44* (23), 12239−12253.
(9) Zhao, Y.; McDonell, V.; Samuelsen, S. Experimental assessment of the combustion performance of an oven burner operated on pipeline natural gas mixed with hydrogen. *Int. J. Hydrogen Energy* **2019**, *44* (47), 26049−26062.
(10) Zhan, X. Y.; Chen, Z. G.; Qin, C. K. Effect of hydrogen-blended natural gas on combustion stability and emission of water heater burner. *Case Stud. Therm. Eng.* **2022**, *37*, 102246.
(11) Kong, Y. Y.; Li, Y. X.; Wang, S. L.; Han, H.; Duan, P. F.; Yu, X. R.; Han, J. K. Experimental study on jet fire characteristics of hydrogen-blended natural gas. *Int. J. Hydrogen Energy* **2023**.
(12) Donohoe, N.; Heufer, A.; Metcalfe, W. K.; Curran, H. J.; Davis, M. L.; Mathieu, O.; Plichta, D.; Morones, A.; Petersen, E. L.; Güthe, F. Ignition delay times, laminar flame speeds, and mechanism validation for natural gas/hydrogen blends at elevated pressures. *Combust. Flame* **2014**, *161* (6), 1432−1443.
(13) Li, Y. C.; Bi, M. S.; Li, B.; Zhou, Y. H.; Gao, W. Effects of hydrogen and initial pressure on flame characteristics and explosion pressure of methane/hydrogen fuels. *Fuel* **2018**, *233*, 269−282.
(14) Ennetta, R.; Alaya, M.; Said, R. Numerical Study of Laminar Flame Velocity of Hydrogen-Enriched Methane Flames Using Several Detailed Reaction Mechanisms. *Arabian J. Sci. Eng.* **2017**, *42* (5), 1707−1713.
(15) Lu, J.; Fu, Z. G.; Liu, J.; Pan, W. G. Influence of air distribution on combustion characteristics of a micro gas turbine fuelled by hydrogen-doped methane. *Energy Rep.* **2022**, *8*, 207−216.
(16) Pan, H. J. T.; Geng, S. J.; Yang, H.; Zhang, G. H.; Bian, H.; Liu, Y. H. Influence of H2 blending on NOx production in natural gas combustion: Mechanism comparison and reaction routes. *Int. J. Hydrogen Energy* **2023**, *48* (2), 784−797.
(17) Metcalfe, W. K.; Burke, S. M.; Ahmed, S. S.; Curran, H. J. A Hierarchical and Comparative Kinetic Modeling Study of C_1 - C_2 Hydrocarbon and Oxygenated Fuels. *Int. J. Chem. Kinet.* **2013**, *45* (10), 638−675.
(18) Gimeno-Escobedo, E.; Cubero, A.; Ochoa, J. S.; Fueyo, N. A reduced mechanism for the prediction of methane-hydrogen flames in cooktop burners. *Int. J. Hydrogen Energy* **2019**, *44* (49), 27123−27140.
(19) Liu, X. Z.; Zhu, G. Y.; Asim, T.; Mishra, R. Combustion characterization of hybrid methane-hydrogen gas in domestic swirl stoves. *Fuel* **2023**, *333*, 126413.
(20) Peng, Q.; Ye, J. H.; Tu, Y. J.; Yang, W. M. E.; J, Q.; Kang, Z.; Fu, G. Experimental and numerical investigation on premixed H_2/C_3H_8/air combustion and thermal performance in a burner with partially filled porous media br. *Fuel* **2022**, *328*, 125227.
(21) Bubnovich, V.; Hernandez, H.; Toledo, M.; Flores, C. Experimental investigation of flame stability in the premixed propane-air combustion in two-section porous media burner. *Fuel* **2021**, *291*, 120117.
(22) Hoda, S. N.; Gandjalikhan Nassab, S. A.; Ebrahim, J. J. Three dimensional numerical simulation of combustion and heat transfer in porous radiant burners. *Int. J. Therm. Sci.* **2019**, *145*, 106024.
(23) Kıymaz, T. B.; Böncü, E.; Güleryüz, D.; Karaca, M.; Yılmaz, B.; Allouis, C.; Gökalp, İ. Numerical investigations on flashback dynamics of premixed methane-hydrogen-air laminar flames. *Int. J. Hydrogen Energy* **2022**, *47* (59), 25022−25033.
(24) Fruzza, F.; Lamioni, R.; Tognotti, L.; Galletti, C. Flashback of H2-enriched premixed flames in perforated burners: Numerical prediction of critical velocity. *Int. J. Hydrogen Energy* **2023**, *48* (81), 31790−31801.
(25) Arrieta, C. E.; García, A. M.; Amell, A. A. Experimental study of the combustion of natural gas and high-hydrogen content syngases in a radiant porous media burner. *Int. J. Hydrogen Energy* **2017**, *42* (17), 12669−12680.
(26) Gao, H. B.; Qu, Z. G.; Feng, X. B.; Tao, W. Q. Methane/air premixed combustion in a two-layer porous burner with different foam materials. *Fuel* **2014**, *115*, 154−161.
(27) Jia, Z. Z.; Ye, Q.; Wang, H. Z.; Li, H.; Shi, S. L. Numerical Simulation of a New Porous Medium Burner with Two Sections and Double Decks. *Processes* **2018**, *6* (10), 185.
(28) Lamioni, R.; Bronzoni, C.; Folli, M.; Tognotti, L.; Galletti, C. Impact of H2-enriched natural gas on pollutant emissions from domestic condensing boilers: numerical simulations of the combustion chamber. *Int. J. Hydrogen Energy* **2023**, *48* (51), 19686−19699.
(29) Ueda, A.; Nisida, K.; Matsumura, Y.; Ichikawa, T.; Nakashimada, Y.; Endo, T.; Kim, W. Effects of hydrogen and carbon dioxide on the laminar burning velocities of methane-air mixtures. *J. Energy Inst.* **2021**, *99*, 178−185.
(30) Yan, Y. F.; Zhang, C. H.; Wu, G. E.; Feng, S.; Yang, Z. Q. Numerical study on methane/air combustion characteristics in a heat-recirculating micro combustor embedded with porous media. *Int. J. Hydrogen Energy* **2022**, *47* (48), 20999−21012.
(31) Ma, P.; Tang, Z.; Cai, W. An experimental study and modeling on the flow resistance of airflow through foam ceramic. *Nat. Gas Ind.* **2010**, *30* (11), 97.
(32) Kuwahara, F.; Yamane, T.; Nakayama, A. Large eddy simulation of turbulent flow in porous media. *Int. Commun. Heat Mass Tran.* **2006**, *33* (4), 411−418.
(33) Hou, C. C.; Zou, L. L.; Sun, L. M.; Zhang, K. X.; Liu, Z.; Li, Y. W.; Li, C. X.; Zou, R. Q.; Yu, J. H.; Xu, Q. Single-Atom Iron Catalysts on Overhang-Eave Carbon Cages for High-Performance Oxygen Reduction Reaction. *Angew. Chem., Int. Ed.* **2020**, *59* (19), 7384−7389.
(34) Chen, X.; Long, S. C.; He, L. X.; Wang, C. X.; Chai, F.; Kong, X. Z.; Wan, Z. M.; Song, X. X.; Tu, Z. K. Performance evaluation on thermodynamics-economy-environment of PEMFC vehicle power system under dynamic condition. *Energy Convers. Manage.* **2022**, *269*, 116082.
(35) GB 17905-2008 Safety management regulation of gas-burning appliances for domestic use.
(36) Huang, X.; Christopher, B.; Chai, S. M.; Xie, X. F.; Luo, S. Z.; Liang, S. Q.; Pan, A. Q. Cowpea-like N-Doped Silicon Oxycarbide/Carbon Nanofibers as Anodes for High-Performance Lithium-Ion Batteries. *ACS Appl. Energy Mater.* **2021**, *4* (2), 1677−1686.
(37) Chen, J. *Exploring New Developments in the Gas Water Heater Industry in the Stock*, Home Appliance: China, 2023.

https://doi.org/10.1021/acsomega.3c07418
ACS Omega 2023, 8, 48370−48380